FLAW PROPAGATION AND BUCKLING IN CLAY-BEARING SANDSTONES

Timothy P. Wangler[1,2], Alisa Stratulat[3], Philippa Duffus[4], Jean H. Prévost[5], George W. Scherer[5]

[1]ETH Zürich, Institute for Technology in Architecture, Zürich, CH

[2]Empa Swiss Federal Institute for Materials Testing and Research, Dübendorf, CH

[3]University of Oxford, Department of Materials, Oxford, UK

[4]University of Oxford, Department of Materials, Oxford, UK

[5]Princeton University, Department of Civil and Environmental Engineering, Princeton, NJ 08544 USA

ABSTRACT

Many historically and culturally significant buildings have sandstones that contain swelling clay inclusions in the binding phase. Differential strains that evolve during wetting and drying cycles can generate stresses that are on the order of the strength of the stone, leading to degradation. Most damage observed in the field is surface delamination and buckling of the stone over a flaw, indicating that the damage is occurring during wetting. Classical buckling theory predicts buckling to occur at a particular aspect ratio, or flaw size. The results of this study confirm buckling theory experimentally. However, the critical flaw size for buckling is so large, that such flaws would not be likely in the original building stone. Through simulation and experiment, the study then explores a potential flaw propagation mechanism whereby nonuniform wetting patterns generate stress intensities capable of flaw propagation. As a result, small flaws can grow and coalesce into a flaw large enough to allow buckling during wetting of the stone.

Keywords: clay, buckling, flaw propagation, stress, hygric swelling, finite element analysis

INTRODUCTION

The problem of conservation of historically and culturally significant monuments and buildings has led to a closer examination of specific mechanisms leading to weathering of the stone components, such as salt crystallization, freezing, and biological attack (Scherer et al. 2001). Another damage mechanism arises with sandstones that have swelling clay inclusions in the binding phase, where stresses on the order of the strength of the stone can arise due to differential wetting and drying. The problem of swelling clays in conservation has been recognized by a number of authors previously (Rodriguez-Navarro 1997, Delgado Rodrigues 2001), and continues to generate interest in recent years (Franzini et al. 2007, Sebastián et al. 2008). It has been demonstrated that the expansion of Portland brownstone results from intracrystalline swelling of mixed-layer chlorite/smectite clays in the cementing phase by incorporation of as many as 4 layers of water molecules (Wangler and Scherer, 2008). Wendler et al. (1990) and Félix (1995) showed the importance of recognizing this problem when coupled with consolidation strategies, as swelling clays can eliminate the effectiveness of a consolidant within just a few wetting cycles. To prevent swelling, Wendler et al. (1990) proposed the use of α,ω-diaminoalkanes; Wangler and Scherer (2009) confirmed that these molecules intercalate into the clay and prevent subsequent invasion by water. The effectiveness of this treatment has been demonstrated in the field (Wendler et al., 1996).

Jiménez-González and Scherer (2004) studied the mechanics and swelling behavior of some clay-bearing sandstones, showing that the properties of the stone change in the wet state and also demonstrating that these stones behave viscoelastically. They developed a novel warping experiment that demonstrates the magnitude of the stresses evolved and provides a useful test to extract some key material properties (Scherer and Jiménez-González, 2005). Additionally, Jiménez-González et al. (2008) analyzed the problem of uniform wetting of a stone block in a wall to show that the maximum stress that could develop during drying or wetting is

$$\sigma_{d/w} = \pm \frac{E_{d/w}}{1 - \nu_{d/w}} \varepsilon_s \tag{1}$$

where $\sigma_{d/w}$ is the drying or wetting stress in the stone, $E_{d/w}$ is the Young's modulus of the dry or wet stone, ε_s is the free swelling strain, and $\nu_{d/w}$ is Poisson's ratio of the dry or wet stone,

usually estimated to be 0.25. The stress is positive (tensile) during drying and negative (compressive) during wetting, and the analysis assumes that the stone is fully wet or dry before the beginning of a cycle. Given that a stone is much weaker in tension than in compression, one would expect to see drying damage resembling mud cracking in the field; however, stones rarely become fully saturated during rainstorms. Although Jiménez-González et al. demonstrated that drying damage can be observed on protrusions that can become fully wetted (2008), the most commonly observed damage in the field is that of buckling and surface delamination, as seen in Figure 1. This damage mode has been observed over various length scales, and requires a preexisting flaw (provided by salt crystallization, freezing, or flaws inherent to the stone itself). It is the goal of this present study to verify buckling damage experimentally and to use finite element simulations to guide an experimental study of a potential flaw propagation mechanism.

THEORY

Buckling is a damage mode characterized by the sudden deformation of a slender structural member due to the buildup of compressive strain energy. For a swelling stone, this can be imagined as the suppression of the free swelling strain ε_s of a thin layer of stone over a flaw where there is no cohesion, as depicted in Figure 2. The flaw is at a depth t below the exterior surface and the width of the flaw is $2b = L$. From classical buckling theory (Hutchinson, 1996), buckling for this geometry occurs when the compressive stress, σ, in the plane of the film,

$$\sigma = \frac{E\,\varepsilon_s}{1-\nu^2} \tag{2}$$

is equal to the critical buckling stress, σ_c,

$$\sigma_c = \frac{E}{1-\nu^2}\frac{\pi^2}{3A_c^2} \tag{3}$$

where E is Young's modulus, ν is Poisson's ratio, and A_c is the critical aspect ratio L/t where buckling occurs. Setting (2) and (3) equal to each other, the critical aspect ratio can then be defined in terms of the free swelling strain:

$$A_c = \frac{\pi}{\sqrt{3\varepsilon_s}} \tag{4}$$

Thus it is possible to determine the critical buckling aspect ratio of a stone if the free swelling strain is known. Swelling clay-bearing sandstones often have free swelling strains between 0.1-3.0 mm/m, meaning typical values for A_c are expected to vary from 30-180. For a circular flaw of radius b, the critical buckling stress was calculated numerically by Hutchinson et al. (1992) and the calculated critical aspect ratio differs from (4) by approximately 9%. For the purposes of this study, the two geometries are considered to be similar enough so that there is no distinction made between the two, with the flaw length of L (in the rectangular case) or twice the radius b (in the circular case) being used interchangeably.

In the present study, the effects of nonuniform wetting patterns are demonstrated to be of significance. An analysis of a similar geometry to that presented in Figure 2 (thin axisymmetric plate with radius b, thickness t, that is clamped at the boundary) taken from Bloom and Coffin (2000) indicates that deflection of the plate can occur at subcritical aspect ratios, if the wetting pattern is not uniform. The upward deflection, w, normalized by the depth to the flaw, is

$$\frac{w}{t} = A^2 \varepsilon_s (1+\nu)\Omega(u) \tag{5}$$

and the bending moment of the plate, M_r, is

$$M_r = -E\,\varepsilon_s\, t^2 \mu(u) \tag{6}$$

where $u = r/b$ is the normalized radial coordinate. The derivations of (5) and (6) are provided in the Appendix. The functions $\Omega(u)$ and $\mu(u)$ depend on the wetting distributions; they are nonzero only if the wetting varies in depth and radius. That is, uniform wetting of a subcritical plate causes in-plane compression, but no deflection; however, nonuniform wetting, such as might result from rain drops on a surface, can cause small deflections. We will show that these deflections can lead to growth of a small sub-surface flaw until it becomes large enough to permit buckling.

MATERIALS AND METHODS

STONE

The stone selected for all studies was Portage Bluestone obtained from Endless Mountain Quarries (Susquehanna, PA, USA). This particular stone was chosen due to its high swelling strain and ease of cutting when preparing samples with high aspect ratios. Clay-bearing stones are generally anisotropic, so the properties were measured only in the orientations of interest, which for our experiments was parallel to the bedding. The free swelling strain, ε_s , measured by dilatometry was 0.8 mm/m and the Young's modulus E measured by 3-point bending in the wet state was 15 GPa. Poisson's ratio ν was assumed to be 0.25. The critical aspect ratio A_c for this stone is then calculated to be 64 from eq. (4).

BUCKLING

For the buckling experiments, rectangular samples of stone were constrained laterally and vertically by brackets and clamps. A moving stage coupled to a load cell enabled a relatively low and consistent restraining load to be applied to the samples. The distance between the clamps was held constant at approximately 20 cm, thus the aspect ratio was adjusted by varying the thicknesses of the samples from approximately 2-7 mm. A silicone dam was applied to the top edges of the sample and water was applied to the top and allowed to enter the stone via capillarity until saturation. The deflection was monitored by a linear variable differential transducer (LVDT, from Macrosensors, Pennsauken, NJ) and was recorded at saturation. A schematic of this setup can be seen in Figure 3.

SIMULATIONS

Two-dimensional finite element simulations were carried out using Dynaflow™ software (Prévost 1983). A regular rectangular grid of 500 x 50 evenly spaced units was set up with the boundary conditions of a free surface on the top and pinned surfaces (i.e., without displacement or rotation) on the other three sides. A crack was placed at a particular depth below the free surface from which the aspect ratio L/t could be defined, as seen in Figure 4a.

By analogy of hygric and thermal strains, swelling was simulated by the input of a heating pattern. The pattern of most interest was that of a single drop with depth equal to one half of its width, seen in Figure 4b. The drop location, *d*, is determined by the leading edge of the drop. The instantaneous stress intensity at the crack tip was then calculated using a linear elastic fracture mechanics constitutive model (Sukumar and Prévost, 2003; Huang et al. 2003). For all simulations, the properties of wet Portage Bluestone were used.

FLAW PROPAGATION

Experimental studies were carried out to test the results of the simulations. Three thin rectangular stone samples were cut to match the geometry of the simulations, and a small diamond saw was used to place a flaw a certain depth from the top by cutting through the thin slab from both sides. An LVDT was placed at the tip of the crack and a drop of water applied at the location where the simulations indicated the most damaging behavior could be expected. The geometry can be seen in Figure 5. The approximate dimensions for the samples tested were L_{slab} = 60-90 mm, h_{slab} = 25-30 mm, L = 30-35 mm, and t = 2-4 mm, which resulted in tested aspect ratios of approximately 8-12. The slab thicknesses were about 5-6 mm for plane strain conditions.

RESULTS

The results of the buckling experiments are shown in Figure 6a. It can clearly be seen that above the critical aspect ratio of 64, millimeter-scale deflections are recorded, indicating buckling of the specimen. Figure 6b zooms in on the micrometer-scale deflections recorded below the critical aspect ratio.

Simulation results are presented in Figure 7a-d. Initial simulations demonstrated that with a uniform wetting pattern, the stress intensity was close to zero, which is consistent with the prediction of zero deflection in Hutchinson's analysis. However, the Bloom and Coffin analysis indicates that positive deflections can occur if the wetting is not uniform. Therefore, a single droplet pattern was simulated and various parametric studies were performed to determine the drop location where the stress intensity was maximal. Using a single drop size (drop radius = 5) for simplicity and beginning with a crack length of 100 units, the drop

location was first held constant and the crack depth was varied. It can be seen in Figure 7a that there is a maximum that occurs when the drop depth is half of the crack depth, and this behavior is not dependent on the drop location. Next, the crack depth was held static and the drop location was varied; Figure 7b shows that there is a maximum when the drop is offset from the crack tip by one drop radius. After this, the crack depth and the drop location were held static (in the positions noted above for maximum stress intensity) and the crack length was varied, effectively changing the aspect ratio. In Figure 7c, it can be seen that there is a maximum at an aspect ratio of approximately 4, and then the stress intensity decays to a baseline level as the aspect ratio grows. Finally, the effects of droplet size, Young's modulus, and swelling strain are shown on this baseline stress intensity in Figure7d.

The results of a flaw propagation experiment are seen in Figure 8. After the water droplet is applied, the LVDT records a deflection, which upon drying begins to decrease. When the droplet fully dries, a residual deflection remains, indicating the existence of permanent damage. This behavior was repeatable across all samples and on the same sample during the same experiment (as seen in Figure 8). An identical experiment was run on a stone sample of similar geometry with no flaw, and although a deflection was observed during wetting, no residual deflection remained, indicating that no permanent damage occurred in the absence of a flaw.

DISCUSSION

BUCKLING

The results of the buckling experiment demonstrate quite unambiguously that buckling is occurring above the critical aspect ratio, consistent with the predictions from theory. It was difficult to cut very thin samples, so there are fewer data at the high aspect ratios. Additionally, the thin samples would fracture between the restraints after one experiment, making repeated experiments on a single sample impossible. Nevertheless, the magnitudes of the deflections at the high aspect ratios make it evident that buckling has occurred. The critical aspect ratio of 64 is rather high, however, predicting a necessary flaw size of ~20-25 cm for buckling if the flaw is at a depth of 3 mm. This is highly unlikely to be found in the stone naturally; thus, a flaw propagation mechanism is necessary for a flaw to grow to this size. A close examination of the subcritical buckling data in Figure 6b shows deflections on

the order of tens to hundreds of microns; these deflections are too high to be free swelling in the direction perpendicular to the plate thickness. Equation (4), derived from Bloom and Coffin's theory, predicts deflections at the subcritical level on the order of those observed due to nonuniform thermal or hygric loading. Uniform wetting is virtually impossible to achieve experimentally, but it also does not occur naturally (due to random wetting from raindrops), so if the subcritical deflections are indicative of stresses that can propagate cracks, then this is a potential flaw propagation mechanism. According to eq. (5), the deflection is expected to vary with the square of the aspect ratio, and this can be seen roughly in Figure 6b. The scatter in the plot is significant, but the deflection depends heavily on the details of the wetting pattern. Exploration of this as a flaw propagation mechanism led to the finite element simulation studies.

FLAW PROPAGATION

The results of the simulations are important in understanding how nonuniform wetting could lead to flaw propagation. The purpose of the simulations was to make order-of-magnitude estimates of the stress intensities and to develop an understanding of the effects of wetting location and flaw size and depth. The computed stress intensities of 1-5 $MPa \cdot m^{1/2}$ are comparable to the critical stress intensities (or fracture toughnesses) measured for sandstones experimentally, which are on the order of 0.3-2 $MPa \cdot m^{1/2}$ (Atkinson 1987). Of greater interest, however, are the parametric studies, shown in Figure 7, of the single drop wetting pattern. While relative depth, drop size, and material properties all have effects, the greatest influence seems to be the relative distance of the drop from the crack tip. In particular, the most damaging location seems to be a point some distance from the tip that is dependent on the size of the droplet. Using this point to show the behavior of the stress intensity as the aspect ratio increases (in effect, propagating the size of the flaw), there seems to be a baseline, and then the stress intensity goes through a maximum before decaying back to the baseline level. The maximum stress intensities occur for aspect ratios of approximately 3-15. The baseline appears to vary linearly with the material properties and droplet size. It should be noted that this model is for an elastically isotropic material with homogeneous material properties. In reality, the stone is viscoelastic and anisotropic, so this model should be taken only as an experimental guide and no more than an estimation of the potential stress intensities that can be developed.

The simulations were instrumental in understanding qualitatively where to wet a stone sample in a flaw propagation experiment. That experiment demonstrated residual deflection, which is interpreted to result from flaw propagation. That a stone sample with no flaw demonstrated similar expansion, but no residual deflection, is evidence that the residual strain is not behavior inherent to the stone and is indeed from flaw propagation. Because of limitations in sample preparation, it was not possible to generate flaws of smaller aspect ratios, but evidently the tested aspect ratios of approximately 8-12 were enough to show that crack propagation occurs, and are good experimental evidence of this propagation mechanism.

BUCKLING AND FLAW PROPAGATION

Several factors should be taken into account for predicting whether a flaw will propagate to a critical level. The shape of Figure 7c suggests that flaws of a particular size are most susceptible to growth, and depending on the critical stress intensity for a particular stone, these flaws will continue to grow, depending on the wetting event. If these flaws grow large enough and coalesce with each other, they can eventually reach a critical size and allow buckling. The depth of a susceptible flaw is probably dependent on parameters such as the rate at which water enters and spreads within a stone, the kinetics of swelling and softening, and the type of wetting that a stone is subjected to (e.g., raindrops, capillary rise, runoff). Of course, the material properties of the stone, such as swelling strain, modulus, and fracture toughness, are all expected to play important parts. Anisotropy will also greatly influence the damage susceptibility, as the likelihood of finding natural flaws is higher and the fracture toughness is lower along the stone's bedding planes. Finally, this study does not take into account mixed mode fracture, and Mode I and Mode II fracture are both expected to play a role in flaw propagation (Hutchinson et al. 1992). While the simulation studies and flaw propagation experiments show the potential for this damage mechanism, a serious predictive model should take all of these factors, and also the viscoelastic properties of the stone, into account.

An interesting question is whether this mechanism can lead to damage without the aid of a flaw nucleation mechanism, such as salt crystallization or freezing. Figure 7c showed that the most susceptible aspect ratios for flaw growth are ~3-15. This means that flaws on the order of 100-500 μm, which are not unlikely for sandstones with grains in this range, would

be susceptible nucleating sites at depths anywhere from 0.5 to 2 mm deep for an aspect ratio of 4. This would make damage from this mechanism possible without the aid of another damage mechanism.

CONCLUSIONS

The results of this study experimentally confirm a theoretical analysis of the buckling damage commonly observed in swelling sandstones in the field. Theory predicts that flaws exceeding a critical aspect ratio will allow buckling of the overlying layer of stone. This critical aspect ratio, however, is rather high and not expected to be found in natural stones. To account for the presence of such large flaws, we explored the possibility that small flaws grow as a result of nonuniform wetting patterns, which lead to subcritical deflections and bending moments. Finite-element simulations show that stress intensities on the order of the critical stress intensities for sandstone could be generated by a single-drop wetting pattern at a specific location, and that flaws of a particular size appear to be most susceptible to growth. This was tested experimentally, and it was shown that nonuniform wetting results in a residual deflection indicative of crack propagation. Undoubtedly, there are a number of factors that influence the degradation of clay-bearing sandstones, such as salt crystallization and freezing, and this work demonstrates the potential for these stones to degrade with or without the aid of these other mechanisms.

ACKNOWLEDGMENTS

This work was supported in part by Grant MT-2210-07-NC-05 from the National Center for Preservation Technology and Training.

APPENDIX

If an axisymmetric clamped plate of radius b and thickness t (seen in Figure 9) is subjected to a thermal or a hygric stress, the deflection w is given by (Bloom and Coffin, 2001)

$$w = -\left(\frac{b}{K}\right)\left(\frac{1-u^2}{2}\right)\int_0^1 M_T u\,du + \left(\frac{b^2}{K}\right)\int_u^1 \frac{1}{u'}\int_0^{u'} M_T u''\,du''\,du' \tag{7}$$

where $u = r/b$, K is the bending stiffness,

$$K = \frac{E t^3}{12(1-\nu)^2} \tag{8}$$

and M_T is the first moment of the strain

$$M_T = \frac{E}{1-\nu}\int_{-t/2}^{t/2} \varepsilon_f z\,dz = \frac{E\varepsilon_s t_s (t-t_s)}{2(1-\nu)} \tag{9}$$

where $\varepsilon_f = \varepsilon_s$ is the free swelling strain. The depth of the saturated zone is t_s, the upper and lower surfaces of the plates are at $z = t/2$ and $z = -t/2$, respectively, so the wetted depth at a particular z is $t/2 - t_s$. If the normalized thickness of the wet zone is $H(u) = t_s(u)/t$, then eq. (9) can be written as

$$M_T = \frac{E\varepsilon_s t^2}{2(1-\nu)} H(u)\left[1 - H(u)\right] \tag{10}$$

Defining the aspect ratio of the plate as $A = b/t$, the normalized deflection is

$$\frac{w}{t} = A^2 \varepsilon_s (1+\nu)\Omega(u) \tag{11}$$

where

$$\Omega(u) = 6\left[\left(1-u^2\right)\int_0^1 \left[1 - H(u)\right]H(u)u\,du + \int_u^1 \frac{1}{u'}\int_0^{u'} \left[1 - H(u'')\right]H(u'')u''\,du''\,du'\right] \tag{12}$$

It is seen from eq. (12) that when $t_s = t$ then $H(u) = 1$, meaning $\Omega(u) = 0$ and therefore $w = 0$, so there will be no deflection in the plate when it is uniformly wet.

From the same analysis, the bending moment M_r in the plate is

$$M_r = -(1+\nu)\int_0^1 M_T u\,du - \left(\frac{1-\nu}{u^2}\right)\int_0^u M_T\,u\,du \;=\; -E\,\varepsilon_s\,t^2\,\mu(u) \tag{13}$$

where

$$\mu(u) = \frac{1}{2}\left(\frac{1+\nu}{1-\nu}\right)\int_0^1 H(u)\left[1-H(u)\right]u\,du + \left(\frac{1}{2u^2}\right)\int_0^u H(u)\left[1-H(u)\right]u\,du \tag{14}$$

Again, it can be seen that if the wetting distribution is uniform (H = 1), then the bending moment M_r will also be zero.

FIGURES

a)

b)

Figure 1: Buckling damage commonly observed for swelling clay-bearing sandstones. Photos of damage to Portland Brownstone on Victoria Mansion, Portland, ME (photo by author). (a) Buckling below mortar joint between ashlars; (b) large-scale buckling of wall.

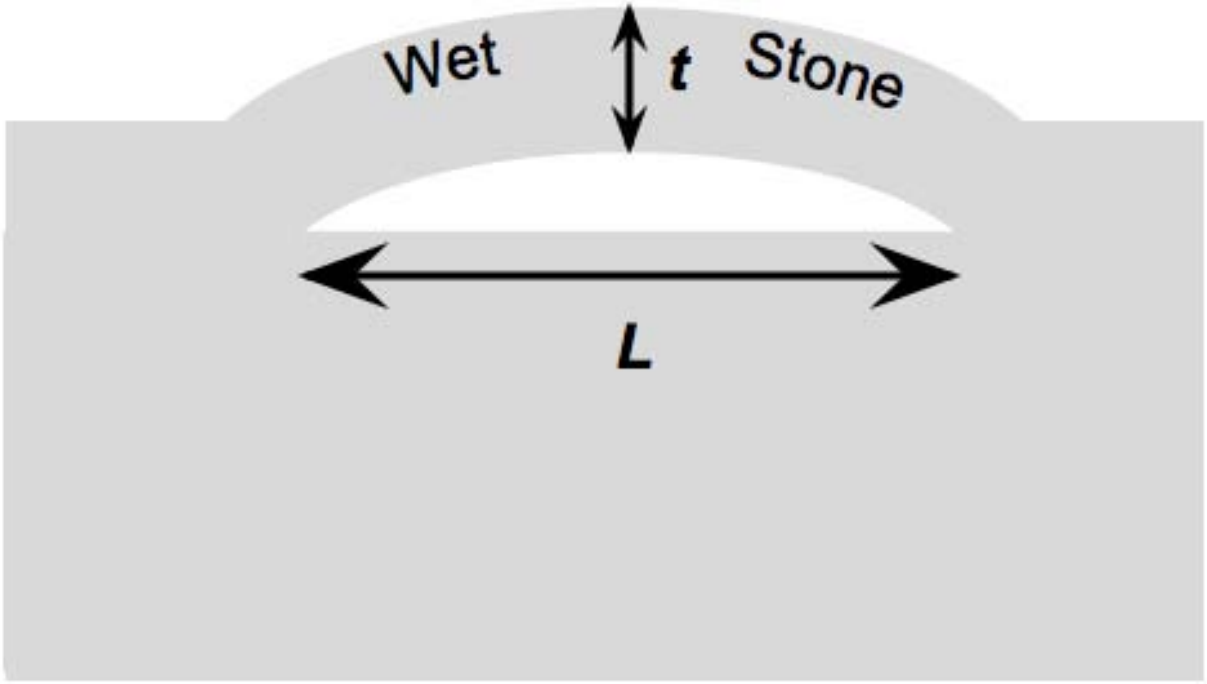

Figure 2: Schematic of buckling problem. A flaw of size L is at a depth t below the surface of the stone, and the wet stone above the flaw is attempting to swell while the bulk of the stone around it suppresses the expansion. If L/t is above the critical aspect ratio $(L/t)_{crit}$, then buckling is expected.

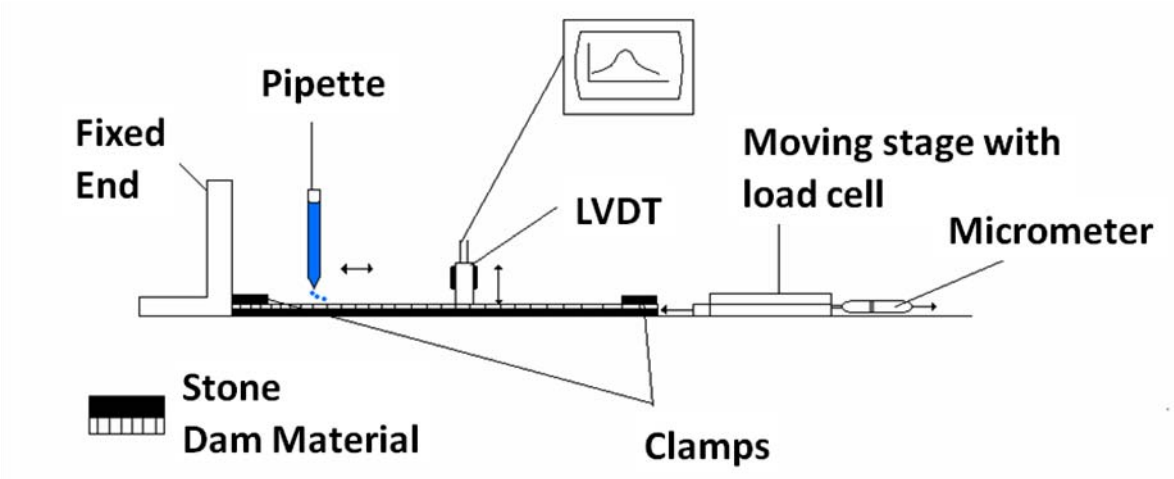

Figure 3: Schematic of buckling experimental setup. Stone slab is fixed at the ends by clamps and brackets. A moving stage with load cell is used to keep the initial restraining force on the sample constant. LVDT at center monitors displacement, and sample's wetting is controlled by a pipet and a dam. From Duffus (2007).

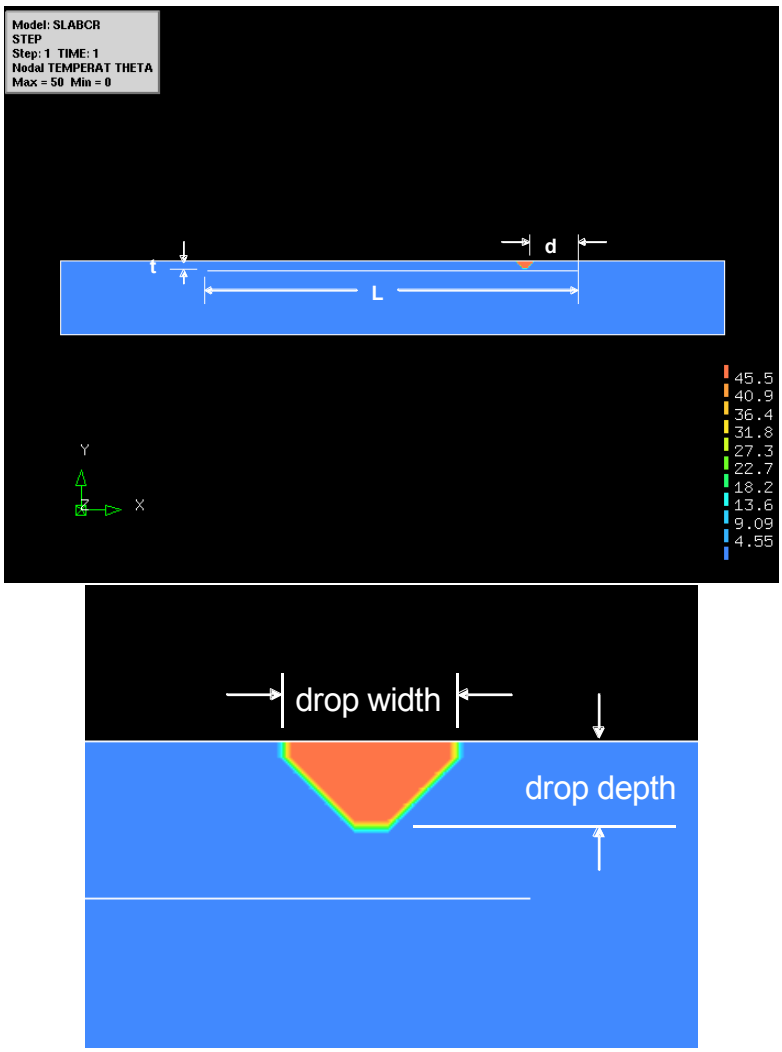

Figure 4a-b: Geometry of finite element simulation model. Boundary conditions are: top surface free and all sides pinned. Important dimensions for the stone model (top) and the droplet wetting pattern (bottom) are noted. The drop depth, *d*, for all simulations was equal to one half the drop width.

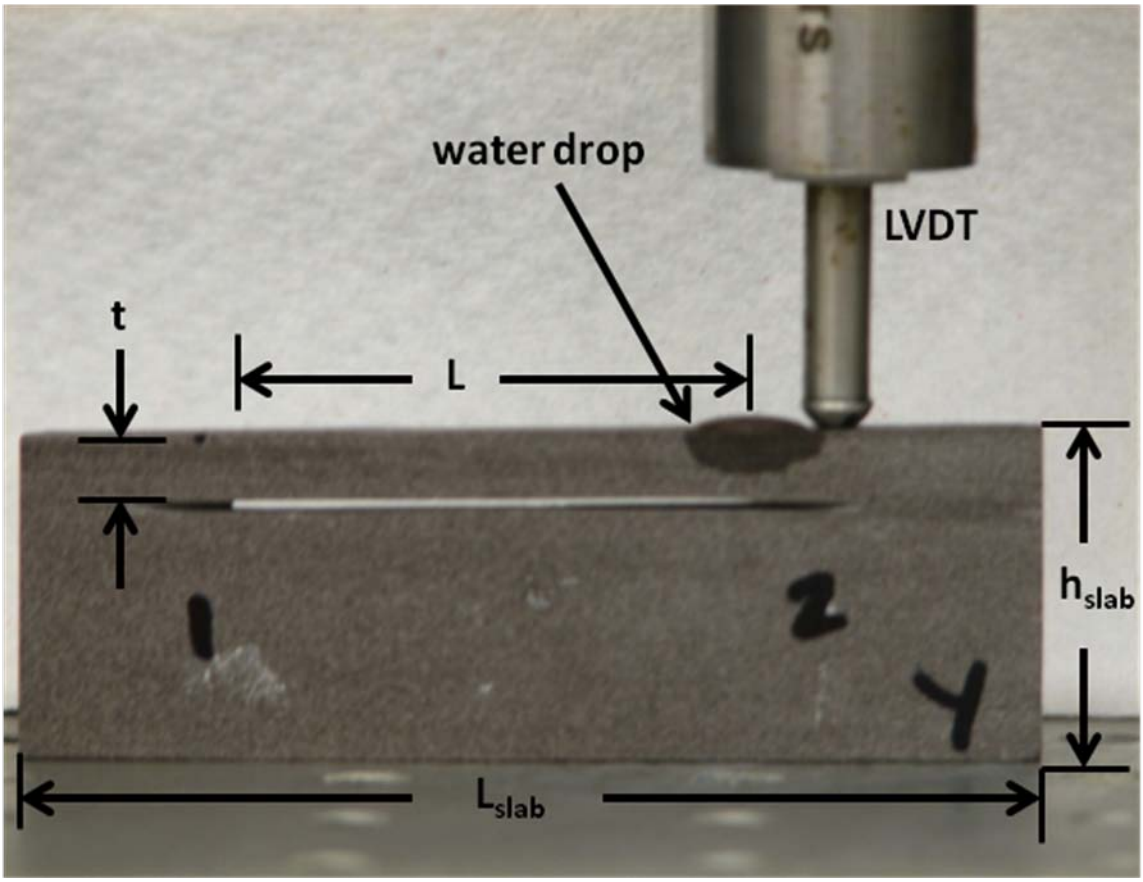

Figure 5: Photo of sample used for flaw propagation experiment, with dimensions indicated.

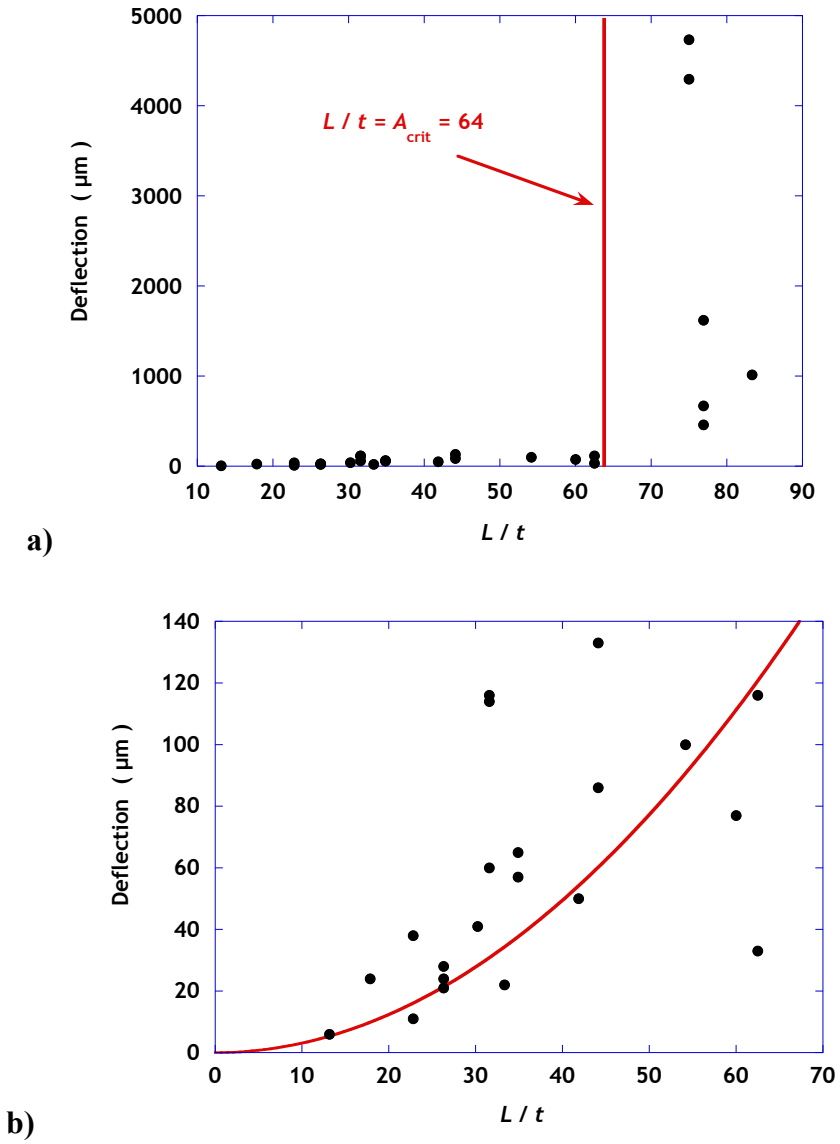

Figure 6: a) Plot of deflection versus aspect ratio for buckling experiments (top). Data show millimeter-scale deflections above the critical aspect ratio, indicating buckling. b) Plot of subcritical deflection versus aspect ratio for buckling experiments (bottom). Data show deflections on the order of tens to hundreds of microns, and approximately parabolic dependence on aspect ratio.

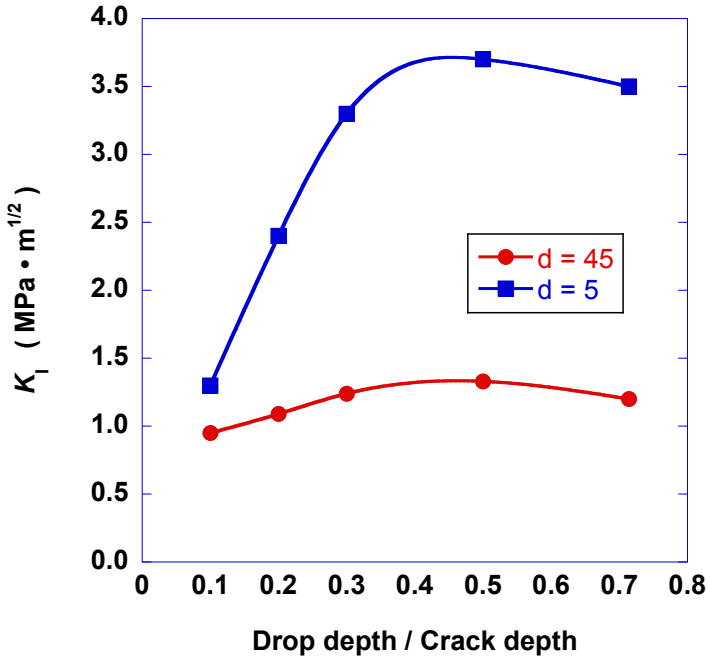
4.0
3.5
3.0
2.5
2.0
1.5
1.0
0.5
0.0
0
0.1
0.2
0.3
0.4
0.5
0.6
0.7
0.8
K_I (MPa • $m^{1/2}$)
d = 45
d = 5
Drop depth / Crack depth

a)

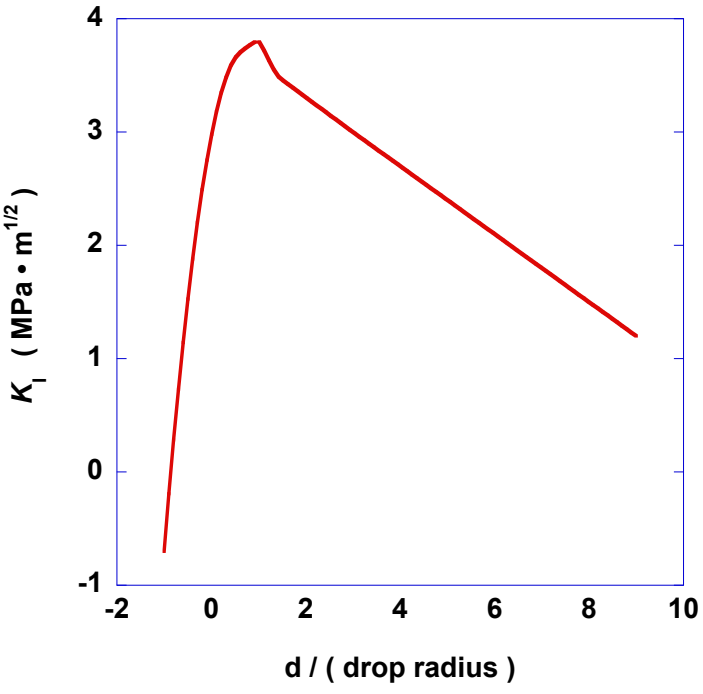
4
3
2
1
0
-1
-2
0
2
4
6
8
10
K_I (MPa • $m^{1/2}$)
d / (drop radius)

b)

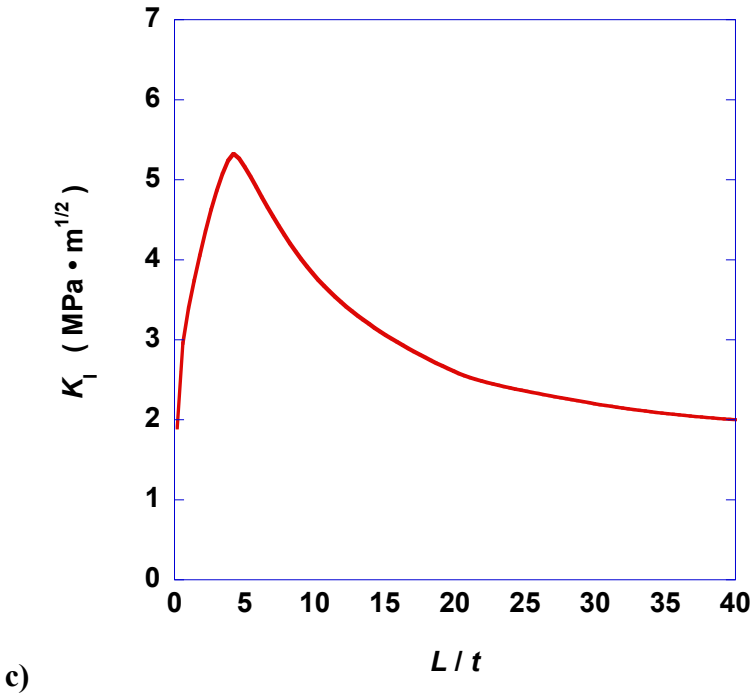

c)

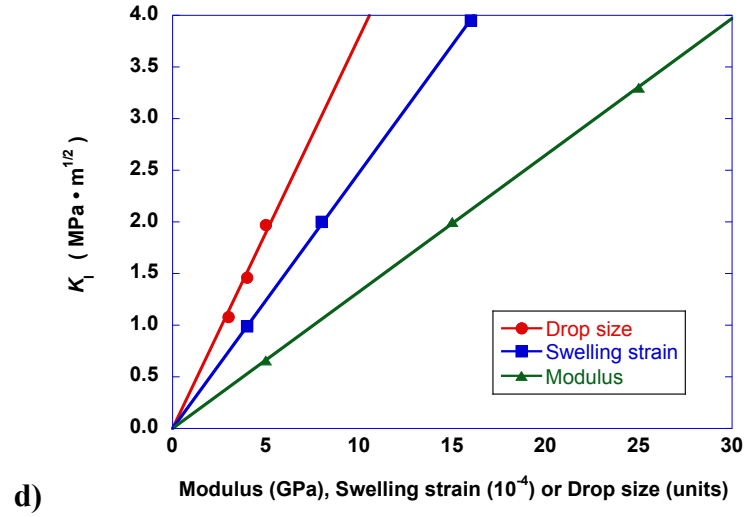

d)

Figure 7. Results of finite element simulations. (a) Varying crack depth relative to drop depth produces a maximum when the drop depth is one half the crack depth, irrespective of drop location *d* (top). (b) Holding crack depth constant at this location and varying drop location *d*, a maximum is observed when the drop location is one drop radius from the edge of the crack (second from top). Negative stress intensities when drop location is past the crack tip indicate compression. (c) Holding crack depth constant and drop location constant based on the maxima from the previous two plots, increasing the aspect ratio (by increasing crack size, *L*) shows a maximum before decaying to a baseline level. (d) Baseline level of the stress intensity varies approximately linearly with varying material properties and drop size.

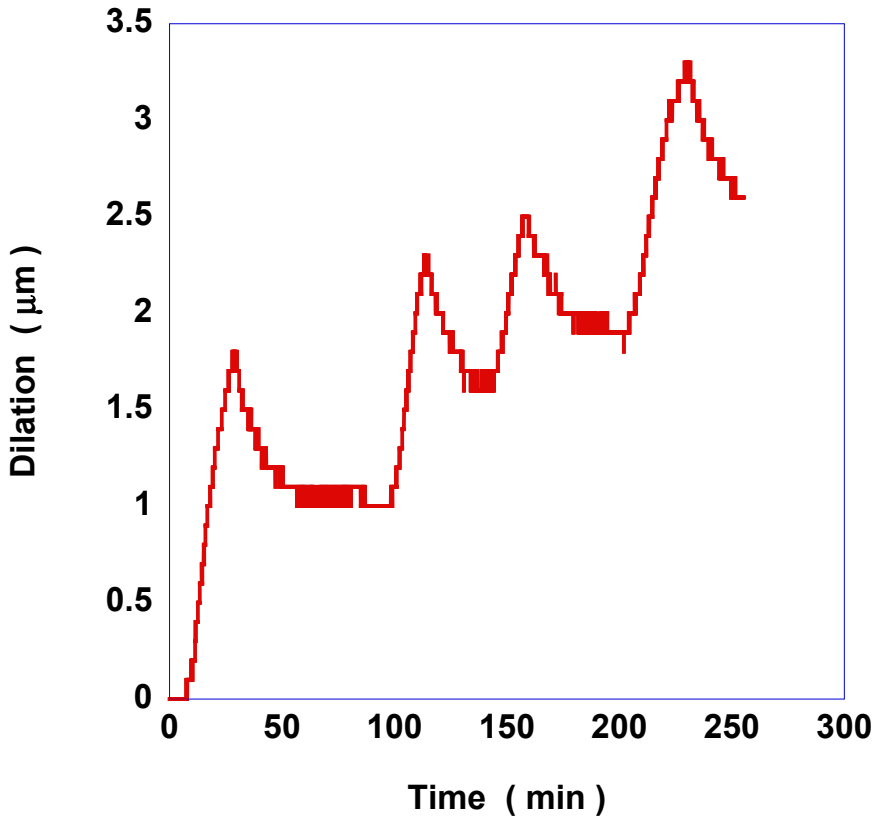

Figure 8. Flaw propagation experiment showing increasing deflection during wetting, decreasing deflection during drying, and residual deflection after drying, indicating crack propagation.

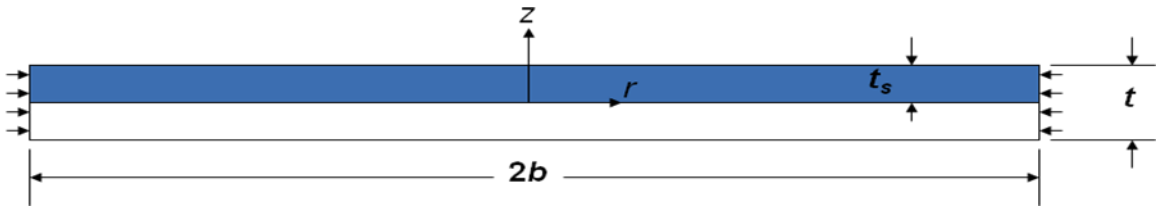

Figure 9. Schematic for analysis of subcritical deflections. Axisymmetric flaw of radius b and thickness t is constrained laterally and vertically on the boundary, origin is at center of the flaw in the r and z dimensions. Wetted depth t_s can be uniform, or can vary across the flaw.

REFERENCES

Atkinson BK (1987) Fracture mechanics of rock. Academic Press, London. p 534.

Bloom F, Coffin, D (2000) Handbook of thin plate buckling and postbuckling. Chapman & Hall/CRC, Boca Raton, FL, USA

Delgado Rodrigues J (2001) Swelling behavior of stones and its interest in conservation. Materiales de Construcción 51(263-264):183-195

Duffus, P (2007) Mechanics of buckling of stones that expand upon exposure to moisture. Masters thesis, University of Oxford, Oxford, UK

Félix, C. (1995) Peut-on consolider les grès tendres du Plateau suisse avec le silicate d'éthyle? (Can one consolidate the soft sandstones of the Swiss plateau with ethyl silicate?), pp. 267-274 in Preservation and restoration of cultural heritage, ed. R. Pancella, Proc. LCP Congress, Montreux

Franzini M, Leoni L, Lezzerini M, Cardelli R (2007) Relationships between mineralogical composition, water absorption and hydric dilatation in the 'Macigno' sandstones from Lunigiana (Massa, Tuscany). Eur J Mineral 19:113–125

Huang R, Sukumar N, and Prévost JH (2003) Modeling Quasi-Static Crack Growth with the Extended Finite Element Method. Part II: Numerical Applications, Int. J. Solids and Structures, 40 (26):7539-7552

Hutchinson JW (1996) Mechanics of Thin Films and Multilayers, Solid Mechanics, Technical University of Denmark, pp. 1-45 (available online at http://www.deas.harvard.edu/hutchinson/)

Hutchinson JW, Thouless MD, Liniger EG (1992) Growth and configurational stability of circular, buckling-driven film delaminations. Acta metall mater 40(2):295-308

Jiménez-González I, Scherer GW (2004) Effect of swelling inhibitors on the swelling and stress relaxation of clay bearing stones. Environ Geol 46:364–377

Jiménez-González I, Rodríguez-Navarro C, Scherer GW (2008) Role of clay minerals in the physicomechanical deterioration of sandstone. J. Geophys. Res. F: Earth Surfaces 113, F02021, doi:10.1029/2007JF000845

Prévost JH (1983) DYNAFLOW: a nonlinear transient finite element analysis programme. Dept. of Civil Engineering, Princeton University, Princeton, NJ USA

Rodríguez-Navarro C, Hansen E, Sebastian E, Ginell W (1997) The role of clays in the deterioration of Egyptian limestone sculptures. J Am Inst Cons 36(2):151–163

Scherer GW, Flatt RJ, Wheeler G (2001) Materials science research for the conservation of sculpture and monuments. MRS Bulletin 26(1):44-50

Scherer GW, Jiménez-González I (2005) Characterization of swelling in clay-bearing stone. In: Turkington AV (ed) Stone decay and conservation SP-390, Geological Soc Am, pp 51–61

Sébastian E, Cultrone G, Benavente D, Fernandez LL, Elert K, Rodríguez-Navarro C (2008) Swelling damage in clay-rich sandstones used in the church of San Mateo in Tarifa (Spain). J Cult Her 9(1):66-76

Sukumar N and Prévost JH (2003) Modeling Quasi-Static Crack Growth with the Extended Finite Element Method. Part I: Computer Implementation, Int. J. Solids and Structures, 40 (26):7513-7537.

Wangler TP, Scherer GW (2008) Clay swelling mechanism in clay-bearing sandstones. Environ Geol 56:529-534

Wangler TP, Scherer GW (2009) Clay swelling inhibition mechanism of α,ω diaminoalkanes in Portland Brownstone. J Mater Res 24(5):1646-1652

Wendler E, Klemm DD, Snethlage R (1990) Consolidation and hydrophobic treatment of natural stone. In: Baker JM, Nixon PJ, Majumdar AJ, Davies H (eds) Proc 5th international conference on durability of building materials and components. Chapman & Hall, London, pp 203–212

Wendler E, Charola AE, and Fitzner B (1996) Easter Island tuff: Laboratory studies for its consolidation, Eighth Int. Congress on Deterioration and Conservation of Stone, ed. J. Riederer, Moller Druck und Verlag, Berlin, pp. 1159-1170